Available online at www.sciencedirect.com
ScienceDirect
Ceramics International 35 (2009) 2959–2963
CERAMICS INTERNATIONAL
www.elsevier.com/locate/ceramint

Characterization of $Ce_{0.9}Gd_{0.1}O_{1.95}$ powders synthesized by spray drying

Peter Blennow [1,*], Weiwu Chen [1,2], Mats Lundberg [1], Mohan Menon [1]

Fuel Cells and Solid State Chemistry Division, Risø National Laboratory for Sustainable Energy, Technical University of Denmark, DK-4000 Roskilde, Denmark

Received 10 December 2008; received in revised form 3 March 2009; accepted 2 April 2009
Available online 24 April 2009

Abstract

$Ce_{0.9}Gd_{0.1}O_{1.95}$ powders were synthesized by spray drying and successive calcinations. The phase purity, BET surface area, and particle morphology of as-sprayed and calcined powders were characterized. After calcination above 300 °C, the powders were single phase and showed a BET surface area of 68 m^2/g when calcined at 300 °C. The conductivity, in air, of sintered pellets was measured by electrochemical impedance spectroscopy (EIS) and it was found to be comparable with literature values. The activation energy for the total conductivity was around 0.83 eV. The powder calcined at lower temperature showed better sinterability and higher total conductivity due to an increased bulk conductivity.

Keywords: A. Powders: Chemical Preparation; D. CeO_2; E. Fuel Cells; E. Electrodes

1. Introduction

Doped CeO_2 possesses many attractive properties which makes it a very promising material for a wide range of applications, such as counter electrodes in opto-electronic devices [1], in high temperature corrosion resistance [2], as automotive three-way catalysts [3], as ultraviolet absorbers [4], oxygen sensors [5] and in solid oxide fuel cells (SOFCs) [6]. In SOFC, for example, $Ce_{0.9}Gd_{0.1}O_{1.95}$ (CGO) is used both in electrolytes and electrodes [6]. Due to its high ionic conductivity at temperatures below 700 °C CGO is an attractive candidate for electrolytes in intermediate-temperature solid oxide fuel cells (IT-SOFCs), especially at temperatures below 600 °C [7]. CGO exhibits high catalytic activity for methane conversion and therefore is an alternative anode material in SOFC for direct methane conversion to avoid carbon deposition in Ni/YSZ anodes [8]. Furthermore, the high oxygen ion conductivity and oxygen reduction activity of CGO make it an attractive candidate for use in composite cathodes in SOFC. The catalytic activity of CGO powders used in the SOFC electrodes depends on the surface area of the powders and is higher for powders with higher specific surface area. In order to produce high surface area CGO powders at relatively low cost, a continuous processing technique with high yield is required.

Ceramic spray drying is a versatile and cheap powder processing method which consists of spraying a water-based suspension of the materials to agglomerate into a stream of heated air [9]. Recently spray drying was used to directly synthesize multi-element ceramic powder from a solution because the resulted powders contain very homogenous chemical compositions with high specific surface area [10,11]. Compared with other chemical synthesis methods, spray drying proved to be a method of high productivity and it is used in variety of industries.

In this work, 10 at.% gadolinium-doped ceria (CGO10) powders with high surface area were synthesized by spray drying and successive calcinations. The phase composition, morphology, size distribution and specific surface area of powders were characterized. The electrical conductivity of sintered CGO10 pellets was examined by electrochemical impedance spectroscopy (EIS) from 300 °C to 700 °C. The effect of calcination temperature on the powder properties was compared as well.

2. Experimental

A 60 wt% CGO10 aqueous nitrate solution containing Ce^{3+} and Gd^{3+} cations in the mole ratio of 9:1 was prepared by

* Corresponding author. Tel.: +45 4677 5868; fax: +45 4677 5858.
E-mail address: pebl@risoe.dtu.dk (P. Blennow).
[1] The authors have made an equal contribution to this article.
[2] Presently at Smart Processing Research Center, Joining and Welding Research Institute, Osaka University, Japan.

0272-8842/$36.00
doi:10.1016/j.ceramint.2009.04.003

dissolving calibrated $Ce(NO_3)_3{\cdot}6H_2O$ (99.9%, Alfa Aesar, Germany) and $Gd(NO_3)_3{\cdot}6H_2O$ (99.9%, Alfa Aesar, Germany) in Millipore® water. The precursor solution was spray dried in a laboratory spray drier (B-290, BÜCHI, Switzerland). The solution was pumped at a flow rate of 60 ml/h with the air flow set at 660 l/h, through a 0.5 mm diameter nozzle. The inlet and the outlet temperatures were set at 220 °C and 145 °C, respectively.

The as-sprayed powders were calcined in a covered alumina crucible in the range of 200–800 °C with a dwell time of 2 h. The powders calcined at 300 °C and 600 °C were further dry ground using an agate mortar and then pressed into pellets, followed by cold isostatic pressing (CIP) at 200 MPa. The pressed pellets were sintered in air between 1200 °C and 1500 °C for 4 h and then cut into appropriate dimensions for conductivity measurements (ca. 0.2 cm thickness, ca. 1 cm in diameter). The density of the sintered pellets was measured by the Archimedes method. The theoretical density of CGO10 was used (7.225 g/cm^3) according to the standard data from JCPDS-00-075-0161. Before measuring the conductivity, Pt-paste was applied as electrodes and the samples were heat treated at 1100 °C for 1/2 h. EIS was used to evaluate the total electrical conductivity and the specific conductivity from grain interiors (gi) and grain boundaries (gb). The measurements were performed in air between 300 °C and 700 °C using an impedance analyzer (Hioki 3532-50, Nagano, Japan) in the frequency range between 1 Hz and 1 MHz.

Thermogravimetric (TG) analysis on as-spray dried CGO10 powder was performed in air at a heating rate of 5 °C/min (STA 409, Netzsch, Germany). The phase composition after heat treatment was determined by powder X-ray diffraction (XRD) using a STOE Theta–Theta diffractometer. X-ray diffractograms were collected at $20^\circ \leq 2\theta \leq 90^\circ$ using Cu K_α radiation. The average grain size d_{avg} was calculated from the XRD diffractograms using Scherrer's Eq. (1):

$$d_{avg} \approx \frac{\kappa\lambda}{\beta\cos\theta} \quad (1)$$

where κ, λ, β, and θ are the shape factor (taken as 0.9), the wave length of the Cu K_α radiation (1.54056 Å), the full width at half maximum (FWHM) of the reflections (corrected for instrument broadening), and the Bragg angle of the specific reflection, respectively. Particle and surface morphology was investigated by scanning electron microscopy (Zeiss Supra35, FEGSEM). Specific surface area (BET) and pore size distribution of the powders were measured with nitrogen adsorption/desorportion (Autosorb1, Quantachrome Instruments, Fl, USA) while particle size distribution of the powders was measured by a laser diffraction particle analyzer (LS100Q, Beckman Coulter Inc., USA). Mei theory was used for calculating the particle size distribution with the real and imaginary part of refractive indices set at 2.2 and 0.1, respectively. Prior to the particle size measurements, the powder was suspended in ethanol and the agglomerates were broken down using an ultrasound treatment.

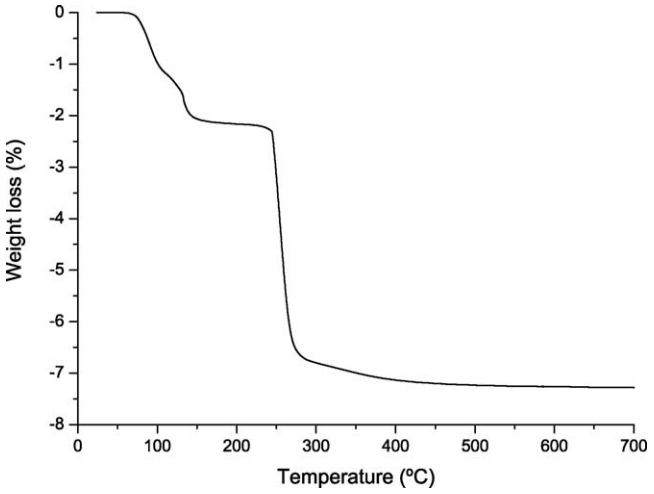

Fig. 1. TG curve of the as-sprayed CGO10 precursor. The data were taken in flowing air at a heating rate of 5 °C/min.

3. Results and discussion

3.1. Powder synthesis and characterization

The precursor solution for synthesis of CGO10 consisted of Ce^{3+}, Gd^{3+}, $(NO_3)^-$, and water. After spray drying, most of the water was removed and a powder-like precursor was formed. The as-sprayed powder contains Ce-, Gd-nitrates and a small amount of residual water. During calcination, the residual water was removed completely, and nitrates decomposed and converted to oxides.

Fig. 1 shows the TG result for as-sprayed powder. There were two major weight loss events present in the curve. The first one started at 80 °C and continued until 110 °C and is associated with the evaporation of residual water from the powder. The second weight loss started at 230 °C and continued until 450 °C. This weight loss is associated with the decomposition of the nitrates. Therefore, a CGO10 phase is expected to form between these temperatures. Fig. 2 shows the

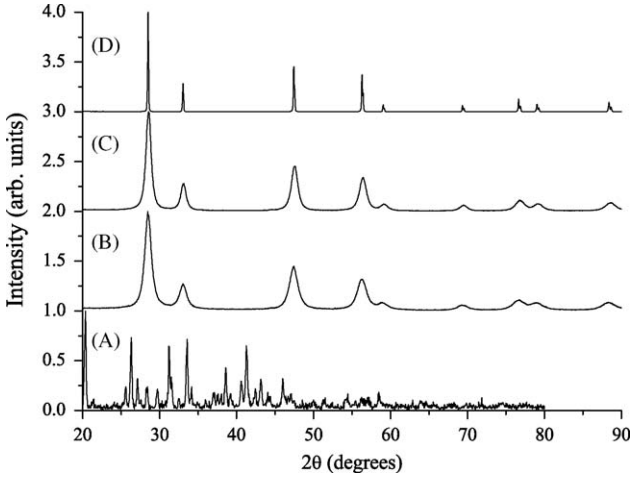

Fig. 2. XRD patterns of (A) as-sprayed CGO10 precursor. (B) After calcination at 300 °C (SD300). (C) After calcination at 600 °C (SD600). (D) After sinter the SD600 powder at 1500 °C.

diffractograms of as-spray dried powder, powders calcined at 300 °C and 600 °C, and the pellets sintered at 1500 °C. As-sprayed powder shows peaks for mainly Ce- and Gd-nitrates. At 300 °C the diffraction pattern shows a single phase powder with a CGO10 composition. This is consistent with the TG curve presented in Fig. 1 where majority of the nitrate decomposition occurred below 300 °C. As the calcination temperature increased, the XRD peaks became slightly narrower and the average crystallite size, calculated with Eq. (1), increased from 9.8 nm after calcination at 300 °C to 13.3 nm after calcination at 600 °C.

The SEM micrograph in Fig. 3 shows crystallites 20–50 nm in size on the agglomerate surface of CGO calcined at 600 °C. From scrutiny of the SEM micrographs of the as-prepared powders supports the results obtained from XRD. The agglomerates observed in the SEM image were usually 10–50 μm in diameter but were easily broken into smaller pieces when mechanical force was applied. The agglomerates are believed to be formed by clustering of small particles assisted by the flowing air during spray drying. Some of these agglomerates break up during calcination at 200 °C due to the water evaporation. According to the TG and XRD results (Figs. 1 and 2) above 300 °C, the nitrates decompose and CGO10 phase starts to form. The agglomerate size increased with increasing calcination temperature.

Fig. 4 shows the adsorption–desorption isotherm for the powder calcined at 300 °C (from here on abbreviated as SD300). Similar isotherms were acquired for the other powders but are not included in this report. The isotherm of all the prepared powders have type IV sorption isotherms [12] with the characteristic hysteresis loop associated with the occurrence of pore condensation typical for mesoporous materials. The hysteresis loop is of H2 character [13] which is often an indication of disordered pores and the distribution of pore size and shape is not well defined. The BET surface area of SD300 was 68.3 m^2/g. The average pore size was 12.1 nm. Fig. 5 shows the particle size distribution of the SD300 and SD600 with a median particle size of 2.8 μm and 7 μm, respectively.

There are various processing techniques available for the preparation of CGO powders, such as homogenous precipitation [14,15], co-precipitation [16,17], combustion synthesis [18], sol–gel [19] and citrate route [20]. These methods provide powders with a wide variety of specific surface area. For example, powders produced by the homogenous precipitation method were reported to have a specific surface area of 120 m^2/g [15]. Other preparation techniques such as combustion synthesis [18], sol–gel [19], soft chemistry routes [21], result in powders with BET surface area below 50 m^2/g. In fact, most of the commercial suppliers such as Rhodia, produce powders with a BET surface area of not more than 40 m^2/g. Synthesis of CGO by co-precipitation method has been scaled up for mass production with a resulting specific surface area of 31.5 m^2/g [22].

However, by using spray drying, as reported in this work, it is possible to fabricate CGO powders that consists of mesoporous particles with a BET surface area of above 50 m^2/g (68.3 m^2/g for SD300) and with particle diameters between 0.5 μm and 3 μm in size. These mesoporous particles are easily agglomerated with a mean particle size of 5 μm. Therefore, spray drying is an attractive method for continuous production of high specific surface area CGO10.

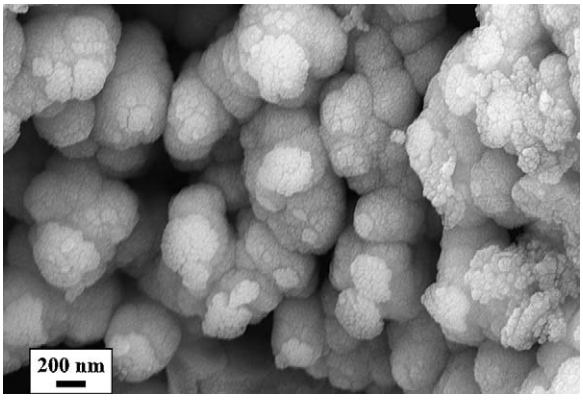

Fig. 3. SEM image showing small particles on the surface of a large agglomerate of CGO calcined at 600 °C. The particles sizes are in the same region as reported from XRD.

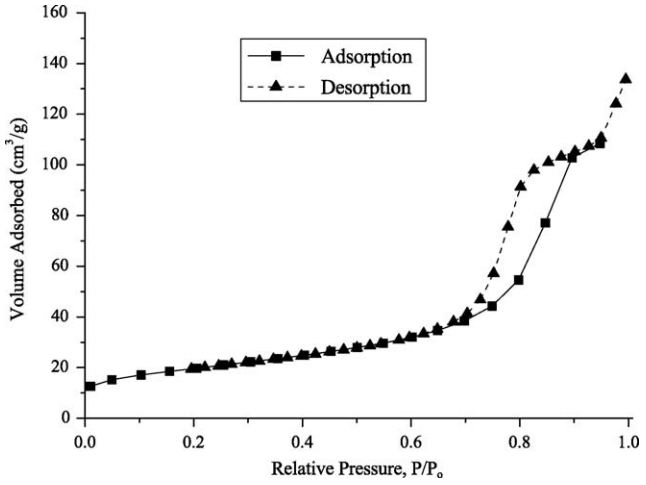

Fig. 4. Nitrogen adsorption/desorption isotherm for SD300 powder.

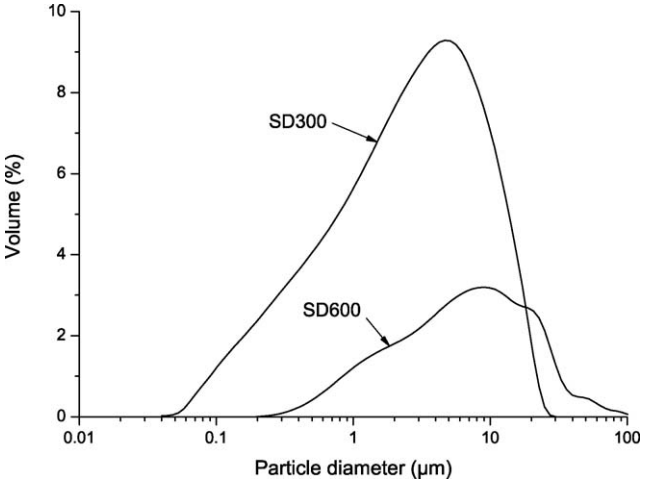

Fig. 5. Particle size distribution of SD300 and SD600 powder measured by laser diffraction.

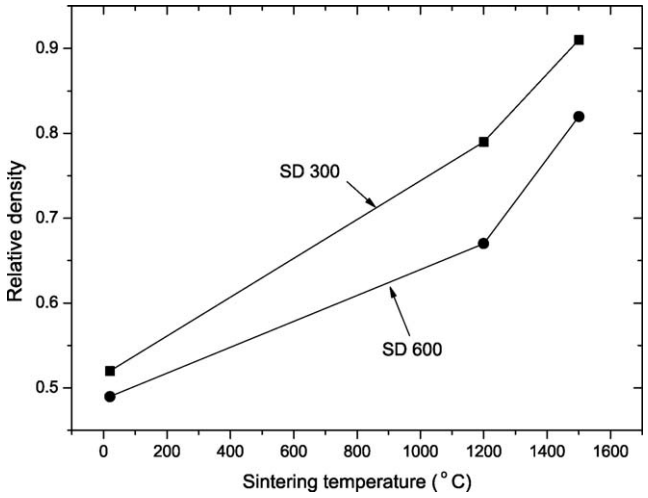

Fig. 6. Densification behavior of SD300 and SD600 powders.

3.2. Sintering and electrical properties

The powders calcined at 300 °C (SD300) and 600 °C (SD600) were selected for sintering and characterization of their electrical properties. Fig. 6 shows the relative density of pellets before and after sintering at 1200 °C and 1500 °C. The SD600 powder had lower green density than the SD300 sample. SD600 samples had lower density than that of SD300 samples at all the sintering temperatures studied here. This could be attributed to the higher agglomerate size in the SD600 powder (see Fig. 5). Furthermore, SD600 had a wider particle size distribution compared to that of SD300, with the distribution shifted towards larger particle size. This should result in a density gradient within the sample resulting in poor sintering. Fig. 7 shows a SEM image of the CGO10 pellets sintered at 1500 °C. The samples were polished and thermally etched at 1400 °C prior to SEM investigation. As can be seen in Fig. 7, the SD300 and SD600 samples sintered at 1500 °C had similar grain size distribution from 1 μm to 3 μm, but the SD600 sample contained more pores with the same size range.

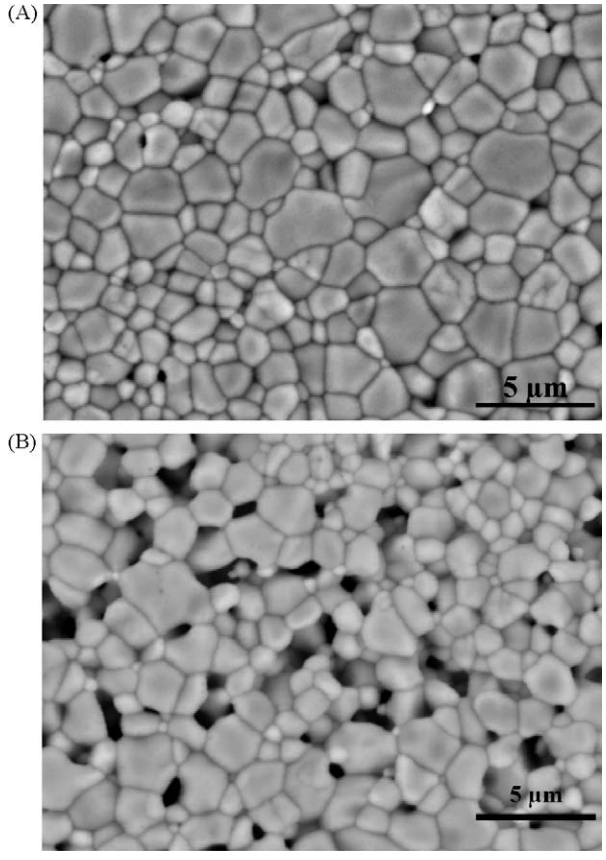

Fig. 7. SEM images of CGO10 pellets sintered at 1500 °C. (A) SD300 as starting powder. (B) SD600 as starting powder.

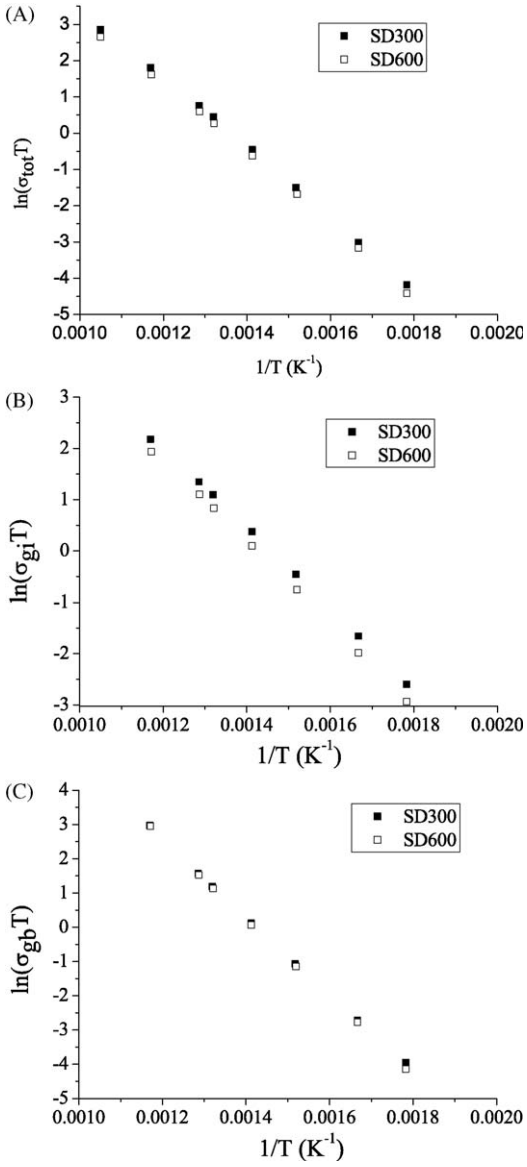

Fig. 8. Arrhenius plots of (A) the total conductivity, (B) the grain interior conductivity, and (C) the grain bulk conductivity of SD300 and SD600 powders sintered in air at 1500 °C.

EIS was performed on the sintered pellets to investigate the electrical conductivity of the sintered samples. Fig. 8 shows the measured electrical conductivity of the grain interiors (gi), grain boundaries (gb) and the total conductivity of the SD300 and SD600 samples sintered at 1500 °C. The SD300 sample

had slightly higher conductivity than the SD600 sample at all measured temperatures. However, that is completely due to the higher grain interior conductivity, which is caused by the higher porosity of SD600 sample after sintering (see Fig. 6). The grain boundary conductivity of the two samples was virtually identical, as would be expected from samples fabricated from the same precursor solution. At 600 °C, the total conductivity of SD300 and SD600 samples reaches 8 mS/cm and 6 mS/cm, respectively. This is similar to what has been reported in the literature for CGO10 [7]. This implies that CGO10 powders produced by spray drying precursor solutions are comparable to commercially available CGO powders.

The apparent activation energy of the sintered CGO samples was calculated using Eq. (2):

$$\sigma T = \sigma_0 e^{-\frac{E_\sigma}{kT}} \quad (2)$$

where σ, T, σ_0, E_σ, and k are the conductivity, absolute temperature, pre-exponential factor, activation energy, and Boltzmann's constant, respectively. The apparent activation energy for SD300 and SD600 was calculated from Eq. (2) and found to be 0.83 eV which is in agreement with the literature [7] confirming the quality of the fabricated powders.

4. Conclusions

The spray drying route has been successfully used to synthesize high surface area CGO10 powders directly from a precursor solution. The as-sprayed powder was virtually a mixture of the various precursor nitrates, and after calcination at 300 °C, the pure CGO10 phase appears. The calcined CGO10 powders contained micron-size and mesoporous particles. The powder calcined at 300 °C shows better sinterability. The activation energy for oxygen ion migration was found to be around 0.83 eV.

References

[1] J. Livage, D. Ganguli, Sol–gel electrochromic coatings and devices: a review, Solar Energy Mater. Solar Cells 68 (3–4) (2001) 365–381.

[2] H. Buscail, P. Sotto, J.P. Larpin, Influence of minor additions to Fe–Mn–Al alloys in an oxidizing environment—role of a cerium oxide modified surface on silicon-containing alloys, Journal de Physique IV 3 (C9) (1993) 309–315.

[3] S.C. Laha, R. Ryoo, Synthesis of thermally stable mesoporous cerium oxide with nanocrystalline frameworks using mesoporous silica templates, Chem. Commun. (2003) 2138–2139.

[4] R.X. Li, S. Yabe, M. Yamashita, S. Momose, S. Yoshida, S. Yin, T. Sato, Synthesis and UV-shielding properties of ZnO- and CaO-doped CeO_2 via soft solution chemical process, Solid State Ionics 151 (1–4) (2002) 235–241.

[5] H.-J. Beie, A. Gnörich, Oxygen gas sensors based on CeO_2 thick and thin films, Sens. Actuators B: Chem. 4 (3–4) (1991) 393–399.

[6] B.C.H. Steele, A. Heinzel, Materials for fuel-cell technologies, Nature 414 (6861) (2001) 345–352.

[7] B. Dalslet, P. Blennow, P. Hendriksen, N. Bonanos, D. Lybye, M. Mogensen, Assessment of doped ceria as electrolyte, J. Solid State Electrochem. 10 (8) (2006) 547–561.

[8] H. Timmermann, D. Fouquet, A. Weber, E. Ivers-Tiffee, U. Hennings, R. Reimert, Internal reforming of methane at Ni/YSZ and Ni/CGO SOFC cermet anodes, Fuel Cells 6 (3–4) (2006) 307–313.

[9] S.J. Lukasiewicz, Spray-drying ceramic powders, J. Am. Ceram. Soc. 72 (4) (1989) 617–624.

[10] I. Van Driessche, B. Schoofs, E. Bruneel, S. Hoste, The effect of processing conditions on the properties of spray dried $Nd_1Ba_2Cu_3O_y$/Ag composite superconductors, J. Eur. Ceram. Soc. 24 (6) (2004) 1823–1826.

[11] H.M. Wu, J.P. Tu, Y.Z. Yang, D.Q. Shi, Spray drying process for synthesis of nanosized $LiMn_2O_4$ cathode, J. Mater. Sci. 41 (13) (2006) 4247–4250.

[12] I. Langmuir, The adsorption of gases on plane surfaces of glass, mica and platinum, J. Am. Chem. Soc. 40 (9) (1918) 1361–1403.

[13] K.S.W. Sing, D.H. Everett, R.A.W. Haul, L. Moscou, R.A. Pierotti, J. Rouquérol, T. Siemieniewsk, Reporting physisorption data for gas/solid systems with special reference to the determination of surface area and porosity (Recommendations 1984), Pure Appl. Chem. 57 (4) (1985) 603–619.

[14] P.L. Chen, I.W. Chen, Reactive cerium(IV) oxide powders by the homogeneous precipitation method, J. Am. Ceram. Soc. 76 (6) (1993) 1577–1583.

[15] J.G. Li, Y. Wang, T. Ikegami, T. Mori, T. Ishigaki, Reactive 10 mol% RE_2O_3 (RE = Gd and Sm) doped CeO_2 nanopowders: synthesis, characterization, and low-temperature sintering into dense ceramics, Mater. Sci. Eng. B 121 (1–2) (2005) 54–59.

[16] Y. Wang, T. Mori, J. Drennan, J. Li, Y. Yajima, Low-temperature synthesis of 10 mol% Gd_2O_3-doped CeO_2 ceramics and its characterization, J. Ceram. Soc. Jpn. 112 (112–1) (2004) S41–S45.

[17] M.J. Godinho, R.F. Goncalves, S. Santos, J.A. Varela, E. Longo, E.R. Leite, Room temperature co-precipitation of nanocrystalline CeO_2 and $Ce_{0.8}Gd_{0.2}O_{1.9-\delta}$ powder, Mater. Lett. 161 (8–9) (2007) 1904–1907.

[18] T. Mokkelbost, I. Kaus, T. Grande, M.A. Einarsrud, Combustion synthesis and characterization of nanocrystalline CeO_2-based powders, Chem. Mater. 16 (25) (2004) 5489–5494.

[19] K. Huang, M. Feng, J.B. Goodenough, Synthesis and electrical properties of dense $Ce_{0.9}Gd_{0.1}O_{1.95}$ ceramics, J. Am. Ceram. Soc. 81 (2) (1998) 357–362.

[20] A. Tsoga, A. Naoumidis, W. Jungen, D. Stöver, Processing and characterisation of fine crystalline ceria gadolinia–yttria stabilized zirconia powders, J. Eur. Ceram. Soc. 19 (6–7) (1999) 907–912.

[21] C. Levy, C. Guizard, A. Julbe, Soft-chemistry synthesis, characterization, and stabilization of CGO/Al_2O_3/Pt nanostructured composite powders, J. Am. Ceram. Soc. 90 (1–3) (2007) 942–949.

[22] E. Suda, E. Mori, K. Murai, B. Pacaud, T. Moriga, Development of mass production of $Ce_{0.9}Gd_{0.1}O_{1.95}$ nanopowder with high-sintering characteristics, J. Ceram. Soc. Jpn. 113 (12) (2005) 793–798.